British Journal of Pharmacology

DOI:10.1111/bph.13340
www.brjpharmacol.org

RESEARCH PAPER

High avidity chimeric monoclonal antibodies against the extracellular domains of human aquaporin-4 competing with the neuromyelitis optica autoantibody, NMO-IgG

Kaori Miyazaki-Komine[1,2†], Yoshiki Takai[3†], Ping Huang[1], Osamu Kusano-Arai[4,5], Hiroko Iwanari[4], Tatsuro Misu[6], Katsushi Koda[7], Katsuyuki Mitomo[7], Toshiko Sakihama[4], Yoshiaki Toyama[2], Kazuo Fujihara[6], Takao Hamakubo[4], Masato Yasui[1,8] and Yoichiro Abe[1,8]

[1]Department of Pharmacology, School of Medicine, Keio University, 35 Shinanomachi, Shinjuku-ku, Tokyo 160-8582, Japan, [2]Department of Orthopaedic Surgery, School of Medicine, Keio University, Tokyo, Japan, [3]Department of Neurology, Tohoku University School of Medicine, 1-1 Seiryomachi, Aoba-ku, Sendai 980-8574, Japan, [4]Quantitative Biology and Medicine, Research Center for Advanced Science and Technology, The University of Tokyo, 4-6-1 Komaba, Meguro-ku, Tokyo 153-8904, Japan, [5]Institute of Immunology Co., Ltd., 1-1-10 Koraku, Bunkyo-ku, Tokyo 112-0004, Japan, [6]Department of Multiple Sclerosis Therapeutics, Tohoku University Graduate School of Medicine, 1-1 Seiryomachi, Aoba-ku, Sendai 980-8574, Japan, [7]Research and Development Division, Perseus Proteomics Inc., 4-7-6 Komaba, Meguro-ku, Tokyo 153-0041, Japan, and [8]Keio Advanced Research Center for Water Biology and Medicine, Keio University, Tokyo, Japan

Correspondence
Yoichiro Abe, Department of Pharmacology, School of Medicine, Keio University, 35 Shinanomachi, Shinjuku-ku, Tokyo 160–8582, Japan.
E-mail: yoabe@a6.keio.jp
[†]These authors equally contributed to this study.

Received
29 October 2014
Revised
15 September 2015
Accepted
18 September 2015

BACKGROUND AND PURPOSE

Most of the cases of neuromyelitis optica (NMO) are characterized by the presence of an autoantibody, NMO-IgG, which recognizes the extracellular domains of the water channel, aquaporin-4. Binding of NMO-IgG to aquaporin-4 expressed in end-feet of astrocytes leads to complement-dependent disruption of astrocytes followed by demyelination. One therapeutic option for NMO is to prevent the binding of NMO-IgG to aquaporin-4, using high-avidity, non-pathogenic–chimeric, monoclonal antibodies to this water channel. We describe here the development of such antibodies.

EXPERIMENTAL APPROACH

cDNAs encoding variable regions of heavy and light chains of monoclonal antibodies against the extracellular domains of human aquaporin-4 were cloned from hybridoma total RNA and fused to those encoding constant regions of human IgG1 and Igκ respectively. Then mammalian expression vectors were constructed to establish stable cell lines secreting mature chimeric antibodies.

KEY RESULTS

Original monoclonal antibodies showed high avidity binding to human aquaporin-4, as determined by ELISA. Live imaging using Alexa-Fluor-555-labelled antibodies revealed that the antibody D15107 more rapidly bound to cells expressing human aquaporin-4 than others and strongly enhanced endocytosis of this water channel, while D12092 also bound rapidly to human

aquaporin-4 but enhanced endocytosis to a lesser degree. Chimeric D15107 prevented complement-dependent cytotoxicity induced by NMO-IgG from patient sera *in vitro*.

CONCLUSIONS AND IMPLICATIONS

We have established non-pathogenic, high-avidity, chimeric antibodies against the extracellular domains of human aquaporin-4, which provide a novel therapeutic option for preventing the progress and recurrence of NMO/NMO spectrum disorders.

Abbreviations

ADCC, antibody-dependent cellular cytotoxicity; AQP4, aquaporin-4; BV, budded baculovirus; CDC, complement-dependent cytotoxicity; ECD, extracellular domain; HRP, horseradish peroxidase; mAb, monoclonal antibody; MS, multiple sclerosis; NMO, neuromyelitis optica; NMOSD, NMO spectrum disorders; OAPs, orthogonal arrays of particles; PFA, paraformaldehyde

Table of Links

TARGETS
Ion channels
AQP4, aquaporin 4

This Table lists key protein targets and ligands in this article which are hyperlinked to corresponding entries in http://www.guidetopharmacology.org, the common portal for data from the IUPHAR/BPS Guide to PHARMACOLOGY (Pawson *et al.*, 2014) and are permanently archived in the Concise Guide to PHARMACOLOGY 2013/14 (Alexander *et al.*, 2013).

Introduction

Neuromyelitis optica (NMO) is an autoimmune disease of the CNS, selectively targeting the optic nerves and the spinal cord, in which a disease-specific autoantibody called NMO-IgG plays a central role (Lennon *et al.*, 2004; Fujihara, 2011; Lucchinetti *et al.*, 2014). The targets of NMO-IgG are the extracellular domains (ECDs) of aquaporin-4 (AQP4), the predominant water channel in cells of the CNS (Lennon *et al.*, 2005). Binding of NMO-IgG to the ECDs of AQP4, which is expressed in the end-feet of astrocytes, leads to complement-dependent disruption of astrocytes followed by demyelination (Fujihara, 2011). Therefore, although NMO is a neuroinflammatory disease of the CNS, similar to multiple sclerosis (MS), the pathomechanism of NMO is completely different from that of MS. Most importantly, several drugs, clinically effective for MS patients, such as interferon β, fingolimod and natalizumab, have no effect on and sometimes actually harm patients with NMO or NMO spectrum disorders (NMOSD) (Jarius *et al.*, 2014; Trebst *et al.*, 2014).

Aquaporin-4, functioning as a tetramer, is a member of the six-transmembrane water channel family. Among this family, AQP4 is one of the members forming supramolecular structures called orthogonal arrays of particles (OAPs), in which AQP4 tetramers are orthogonally arranged (Yang *et al.*, 1996; Furman *et al.*, 2003). AQP4 has two isoforms, M1 and M23, derived from different transcriptional start sites (Lu *et al.*, 1996), which form homo/heterotetramers with any combination of these isoforms. Only M23 has an ability to form OAPs, while M1 does not because its unique intracellular N-terminal region, with 22 extra amino acids, interferes with OAP formation (Suzuki *et al.* 2008). Thus, while M23 homotetramers form huge arrays, little OAP formation of M1 homotetramers can be seen. The mixture of M1/M23 homo/heterotetramers, which is the naturally occurring form in cells endogenously expressing AQP4, shows relatively smaller arrays than the M23 homotetramers (Furman *et al.*, 2003). Several groups, including ours, have reported that epitopes for NMO-IgG, restricted to the ECDs of AQP4, do vary but, in most cases, the NMO-IgGs preferentially recognize AQP4 incorporated into OAPs (Nicchia *et al.*, 2009; Pisani *et al.*, 2011; Crane *et al.*, 2011; Miyazaki *et al.*, 2013; Pisani *et al.*, 2013). These observations indicate that OAP formation of AQP4 is required for certain NMO-IgGs to bind to AQP4, because the primary sequences of the ECDs in the M1 and M23 isoforms are identical.

Recently, we established monoclonal antibodies (mAbs) against the ECDs of human AQP4 (hAQP4) using a baculovirus display method (Saitoh *et al.*, 2007; Miyazaki *et al.*, 2013). These antibodies displaced NMO-IgG binding to AQP4 expressed in CHO cells *in vitro* (Miyazaki *et al.*, 2013). Because binding of NMO-IgG to the ECDs of AQP4 apparently triggers the clinical signs of NMO/NMOSD, administering these antibodies may prevent the progress of NMO. However, the subclasses of these antibodies are either IgG2a or IgG2b, which can induce complement-dependent cytotoxicity (CDC) and antibody-dependent cellular cytotoxicity (ADCC). In addition, administering mouse IgG also induces an immunological response strongly affecting the half-life of the protein and the effectiveness of therapy. In this report, we developed chimeric mAbs whose constant regions of both heavy and light chains were changed to those of non-pathogenic human IgG. They still retained high avidities for AQP4 with EC_{50} values of around 1 nM. In addition, one of them induced a significant level of AQP4 endocytosis, which may sequester the target of NMO-IgGs from the cell surface.

We propose that these chimeric mAbs provide a novel therapeutic option for NMO.

Methods

Establishment of stable CHO cell lines

CHO cells and their derivatives were maintained in Ham's F12 medium supplemented with 10% FBS, 50 units · mL^{-1} penicillin and 50 μg · mL^{-1} streptomycin. The stable CHO cell line expressing hAQP4 M23 alone (hAQP4-M23, Supporting Information Figure S1A, lane 1) was described in Miyazaki *et al*. (2013). To establish CHO cells expressing hAQP4 M1 isoform alone (hAQP4-M1, Supporting Information Figure S1A, lane 2), cDNA encoding hAQP4 M1, whose Met^{23} was changed to Leu (Miyazaki *et al*., 2013) to avoid expression of M23 isoform by a leaky scanning mechanism (Rossi *et al*., 2010), was inserted into the pIRES2-EGFP vector (Clontech Laboratories, Mountain View, CA, USA). To establish CHO cell clones expressing both M1 and M23 isoforms (hAQP4-M1/M23, Supporting Information Figure S1A, lane 3), an expression vector was constructed according to the design shown in Supporting Information Figure S1B. The vectors were digested with AflII to be linearized and transfected into CHO cells seeded onto 35 mm dishes (2×10^5 cells) with Lipofectamine (Life Technologies Corporation, Carlsbad, CA, USA) and Plus reagents (Life Technologies Corporation), followed by selection of G418-resistant clones, as described by Miyazaki *et al*. (2013).

To establish cells secreting the C9401 chimeric mAb, cDNA encoding the chimeric C9401 light chain inserted into the pIRES2-EGFP vector was introduced into CHO cells, and a G418-resistant single clone was isolated as described previously. Then the pEBMulti-Puro vector containing cDNA encoding the chimeric C9401 heavy chain was transfected into the clone expressing the C9401 chimeric light chain and selected with both G418 and puromycin (10 μg · m^{-1}, Wako Pure Chemical Industries, Osaka, Japan). In the case of chimeric D12092 and D15107, the pEBMulti-Puro and PEBMulti-Hyg vectors containing each chimeric heavy and light chains, respectively, were cotransfected into CHO cells and selected with both puromycin and hygromycin B (100 μg · mL^{-1}, Wako Pure Chemical Industries).

Cloning of variable regions of mAbs against the extracellular domains of hAQP4 and construction of chimeric mAbs

Total RNA of hybridoma clones C9401, D12092, D15107 and D15129 was extracted with Isogen (Nippon Gene, Tokyo, Japan). First-strand cDNA was synthesized with SuperScript VILO MasterMix (Life Technologies Corporation) from 2.5 μg of total RNA. To obtain cDNA encoding variable regions of heavy and light chains of each mAb, PCR was performed with KOD-Plus-Neo (Toyobo, Osaka, Japan). The sense primers used for cloning of heavy and light chains are listed in Supporting Information Tables S1 and S2, respectively, designed according to Strebe *et al*. (2010) and Schaefer *et al*. (2010) with slight modification. As for the antisense primers, 5′-ACAGGGGCCAGTGGATAGAC-3′ for Igγ2a (D15107 and D15129), 5′-AGGGGCCAGTGGATAGACTG-3′ for Igγ2b (C9401 and D12092) and 5′-GGATACAGTTGGTGCAGCATC-3′ for Igκ were used. The constant region of human Igκ was also cloned by PCR from genomic DNA of HeLa cells extracted with Wizard Genomic DNA Purification Kit (Promega, Madison, WI, USA) with KOD-Plus-Neo using primers 5′-ACTGTGGCTGCACCATCTGTCTTCATCTTC-3′ and 5′-TCTAACACTCTCCCCTGTTGAAGCTCTTTG-3′. Amplified fragments were treated with 10× A-attachment mix (Toyobo) to add adenine to its 3′ end, followed by subcloning into pGEM-T vector (Promega) for sequencing. The constant region of human Igγ1 was derived from pFUSE-CHIg-hG1e3 vector (InvivoGen, San Diego, CA, USA), to which E233P/L234V/L235A/ΔG236 and A327G/A330S/P331S mutations were introduced to reduce induction of ADCC and CDC.

Nucleotide sequences of obtained fragments were aligned with that of the *Mus musculus* genomic DNA using the basic local alignment search tool (National Center for Biotechnology Information) to identify V gene segments highly homologous with each cDNA (Supporting Information Figure S2). Then sense primers 5′-TCTAACCATGGGATGGAGCTGGATCTTTC-3′ for the heavy chain of C9401; 5′-GAGCCCCCATCAGAGCATGGCTGTC-3′ for the heavy chains of D12092 and D15107 and 5′-TCTCAGAGATGGAGACAGACACACTCCTG-3′ for the light chains of C9401, D12092 and D15107 were designed according to the sequence of exon 1 of each corresponding V gene segment of C57BL/6 genome to obtain full-length cDNAs encoding each variable region of heavy and light chains (Supporting Information Figure S2). As a result, D15129 was found to be identical with D15107, so we used only D15107 for subsequent experiments.

To connect each variable region of the heavy chain to the constant region of human IgG1, an NheI site was introduced at the junction of the chimeric heavy chain by PCR using antisense primers 5′-CCGCGGAGCTAGCTGCAGAGACAGTGACCAGAGTC-3′ for C9401 and D15107 and 5′-CCGCGGAGCTAGCTGYAGAGACAGTGACCAGAGTC-3′ for D12092.

To connect each variable region of the light chain to the constant region of human Igκ, an XhoI site was introduced by PCR at the junction of the chimeric light chain using antisense primers 5′-CTCGAGCTTGGTGCCTCCACCGAACGTC-3′ for C9401, 5′-CTCGAGCTTGGTCCCAGCACCGAACGTG-3′ for D12092 and 5′-CTCGAGCTTTGTCCCCGAGCCGAACGTG-3′ for D15107, and sense primers for Igκ constant region 5′-CTCGAGATCAAACGGACTGTGGCTGCACCATCTGTC-3′ to connect C9401 and D15107 and 5′-CTCGAGCTGAAACGGACTGTGGCTGCACCATCTGTC-3′ to connect D12092.

Obtained cDNAs for each chimeric heavy chain and those for each chimeric light chain were inserted into a pEBMulti-Puro and a pEBMulti-Hyg vector (Wako Pure Chemical Industries), respectively, to establish stable CHO cell lines. The cDNA encoding the C9401 chimeric light chain was also inserted into a pIRES2-EGFP vector as described previously.

Purification of chimeric antibodies

To obtain chimeric antibodies secreted into the culture supernatant, CHO cells stably expressing each antibody were cultured in CD-CHO medium (Life Technologies Corporation)

for a week. Then culture supernatants were collected and concentrated with Amicon Ultra 15 mL 10 k (Merck Millipore, Billerica, MA, USA). Concentrated antibody solution was applied to PD-10 desalting columns (GE Healthcare, Little Chalfont, UK) to change buffer to binding buffer (20 mM sodium phosphate, pH7.0, GE Healthcare) to purify with HiTrap rProtein A FF column (GE Healthcare). Bound antibodies were eluted with elution buffer (100 mM glycine-HCl, pH2.7, GE Healthcare) followed by neutralization with neutralizing buffer (1 M Tris–HCl, pH9.0, GE Healthcare). Purified antibodies were subjected again to PD-10 desalting columns to change the buffer to PBS.

ELISA

Baculovirus and CHO cells expressing AQP4 were immobilized and were seeded, respectively, onto 96-well plates. For baculovirus expressing AQP4, virus particles were suspended in PBS (0.05 mg protein $\cdot$ mL^{-1}) followed by addition to 96-well plates (2.5 μg protein per well). The plates were incubated at 4°C overnight then washed twice with PBS containing 0.05% Tween 20. Washed plates were blocked with 40% Block Ace (DS Pharma Biomedical Co., Ltd., Osaka, Japan) in PBS at room temperature for 1 h then incubated with various concentrations of mAb in 40% Block Ace at 4°C overnight.

CHO cells stably expressing AQP4 were seeded at a density of 1×10^5 cells per well. For binding experiments using fixed cells, cells were fixed with 4% paraformaldehyde (PFA) at 4°C overnight. Fixed cells were washed twice with PBS and blocked with 40% Block Ace at room temperature for 1 h. Cells were incubated with various concentrations of mAb in 40% Block Ace at 4°C overnight.

For binding experiments using live cells, culture medium was changed to a binding buffer containing 5 mM Na HEPES (pH 7.4), 140 mM NaCl, 4 mM KCl, 1 mM $MgCl_2$, 1.25 mM $CaCl_2$, 1 mM NaH_2PO_4, 11 mM glucose and 0.2% BSA. Then cells were incubated with various concentrations of mAb in the binding buffer at 37°C for 1 h. Cells were washed with the binding buffer twice and fixed with 4% PFA at room temperature. Two hours later, cells were washed twice with PBS and blocked with 40% Block Ace.

Bound antibodies were detected by incubation with either HRP-conjugated anti-mouse IgG (1:8000, Sigma, St Louis, MO, USA) for original mAbs or HRP-conjugated anti-human IgG (1:40 000, Thermo Fisher Scientific Inc., Waltham, MA, USA) for chimeric mAbs for 1 h. After washing five times with 0.05% Tween 20 for baculovirus plates and with PBS for cell plates, signals were visualized by incubation with 50 μL of 3, 3', 5 and 5' tetramethylbenzidine (Sigma) for 30 min, followed by 50 μL of Stop reagent (Sigma). To calculate the EC_{50} values of each antibody, absorbance at 450 nm was measured with SpectraMax Paradigm (Molecular Devices, Sunnyvale, CA, USA) and fitted to a four-parameter logistic model.

To measure the concentration of injected chimeric D15107 in serum, sera were diluted 10^4-fold and were subjected to ELISA as described previously. Serially diluted–purified chimeric D15107 was used as a standard. Antibody concentration was calculated by software incorporated in SpectraMax Paradigm.

Live imaging of monoclonal antibodies labelled with fluorescent dye

Each mAb was labelled with Alexa Fluor 555 using Alexa Fluor 555 antibody labelling kit (Life Technologies Corporation) according to the manufacturer's instructions. Subconfluent CHO cell clones seeded onto 3.5 cm glass base dishes (AGC Techno Glass Co., Ltd., Shizuoka, Japan) were incubated with 10 μg $\cdot$ mL^{-1} of Alexa-Fluor-555-labelled C9401, D12092 or D15107 at 37°C up to 3 h under observation with an Olympus FV1000 confocal microscope with 60×/NA1.2 objectives (Olympus, Tokyo, Japan). The cells treated with the labelled mAbs at 37°C for 24 h were also observed. Fluorescence of eGFP expressed in the stable cells and labelled antibodies was detected on excitations at 488 and 543 nm, respectively, and five z-stacks spanning approximately 3 μm were captured.

Western blotting

Western blotting was performed as described previously (Abe *et al*. 2008). To check whether AQP4 undergoes degradation at lysosomes, 100 nM bafilomycin A1 (Merck Millipore), an inhibitor for vacuolar-type H^+-ATPase, which causes inhibition of proteases in lysosomes due to an increase in pH value, was added to culture media, and the cells were incubated for 24 h. Antibodies used were monoclonal anti-AQP4 (E5206, 1:2000, Ramadhanti *et al*. 2013), monoclonal anti-GFP (mFX75, 1:500, Wako Pure Chemical Industries) and HRP-conjugated goat anti-mouse IgG (1:5000, Sigma).

Cytotoxicity assay

To evaluate the cytoprotective effect of chimeric D15107 on NMO-IgG-induced CDC, the CHO cell clone expressing both M1 and M23 (hAQP4-M1/M23) was seeded onto 96-well plates at a density of 2×10^4 cells/well and grown at 37°C overnight. CDC was induced by treating cells for 2 h with 200–500 μg $\cdot$ mL^{-1} purified IgG fraction from patients, reported in Miyazaki *et al*. (2013), in PBS in the presence of 2% rabbit serum (Sigma). The chimeric D15107 was added simultaneously with NMO-IgG and complements to cells to evaluate its cytoprotective effect. Cell mortalities were determined by measuring LDH activities derived from dead cells with the LDH-cytotoxic test Wako (Wako Pure Chemical Industries).

Isolating IgG from NMO patient serum

Ig fraction was obtained from the plasma exchange material of a patient with AQP4-antibody-positive NMO. The use of the patient's plasma for this study complied with the Declaration of Helsinki and was approved by the Ethics Committee of Tohoku University Graduate School of Medicine (no. 2011–74).

Animal experiments

All animal care and experimental procedures complied with the Guidelines for the Care and Use of Laboratory Animals of Keio University and were approved by the Keio University Animal Ethics Committee (09084–7). All studies involving animals are reported in accordance with the ARRIVE guidelines for reporting experiments involving animals (Kilkenny *et al*., 2010; McGrath *et al*., 2010). A total of 27 animals were used in the experiments described here.

Adult female C57BL/6JJcl (12 weeks of age and weighing 19–22 g; CLEA Japan, Inc. Tokyo, Japan) were used in all experiments. The mice were housed in polycarbonate cages (3–4 animals per cage) at 21–22°C under a 12 h light/12 h dark cycle with food and water *ad libitum*.

To verify the safety of chimeric D15107, two kinds of experiments were performed: i.p. injection and intra-cerebral injection of chimeric D15107 to assess its effects on peripheral tissues and the CNS respectively. For i.p. injection, 1 mg of chimeric D15107 in PBS (300 μL) was administered. For controls, 300 μL of PBS was injected i.p. and normal kidneys were isolated from age-matched, untreated mice. Body weight was measured for 9 days before and after the injection. Four days after the injection, mice were deeply anaesthetized with isoflurane and whole blood was collected by cardiac puncture with a 1 mL syringe-23G × 1 in needle set. In other mice at the same time, under anaesthesia with sodium pentobarbital (i.p.) and isoflurane, kidneys were removed after perfusion fixation with 4% PFA, as described in Ramadhanti *et al*. (2013). Some mice were killed on day 1 or day 2 of post-injection to collect whole blood as described above. As for intra-cerebral injection, mice were anaesthetized by a combination of inhaled isoflurane and i.p. sodium pentobarbital (40 $mg \cdot kg^{-1}$; if the anaesthetic effect of sodium pentobarbital was inadequate, dosage was increased up to 64.8 $mg \cdot kg^{-1}$ with careful observation) and mounted onto a stereotactic frame (Physio Tech, Tokyo, Japan). A small incision was made slightly to the right of the midline to expose the injection point. A small hole was drilled into the skull 1 mm posterior and 2 mm lateral to the bregma. A finely calibrated glass capillary was then stereotactically inserted to a depth of 3.0 mm, targeting the posterior limb of the internal capsule. Then chimeric D15107 (2.75 $mg \cdot mL^{-1}$) or E5415A (0.5 $mg \cdot ml^{-1}$) was infused, with 5% human serum (Sigma) as complement, in a total volume of 2 μL over a 5 min period. After injection, the glass capillary was held in place for another 5 min; then it was carefully withdrawn. The scalp was closed with 5/0 Vicryl suture. Four days after injection, brains were removed after perfusion fixation, as described in Ramadhanti *et al*. (2013).

Immunohistochemistry

For immunohistochemistry of mouse brains and kidneys, paraffin-embedded tissue sections were made and stained with anti-AQP4 antibody (H-80, Santa Cruz Biotechnology, Santa Cruz, CA, USA), as described previously (Ramadhanti *et al*., 2013).

Data analysis

Statistical analysis was performed using JMP version 11.0.0 (SAS Institute Inc., Cary, NC, USA). Data were analysed using one-way ANOVA followed by the Tukey–Kramer test.

Results

Binding properties of the mAbs against the extracellular domains of human AQP4

In a previous report, we demonstrated four mAbs against the ECDs of hAQP4, some of which could compete against NMO-IgGs and displace their binding from hAQP4 expressed in CHO cells by treatment, even at 2 h after incubation with NMO-IgG *in vitro* (Miyazaki *et al*., 2013). To evaluate their potential as therapeutic drugs, we first determined their avidities by ELISA using 96-well plates, where budded baculovirus (BV) expressing hAQP4 M23, the immunogen used for development of these antibodies, was immobilized. All mAbs (300 $ng \cdot mL^{-1}$) rapidly bound to hAQP4 M23 expressed on the envelope of BV and almost reached a plateau in 6 h, both at room temperature and at 4°C (Figure 1A and B); thus, we performed subsequent binding experiments at 4°C overnight. The mAbs dose-dependently bound to hAQP4 M23 expressed on BV with high avidity, as estimated with EC_{50} values (Figure 1C and Table 1). Interestingly, in both time course and concentration-dependent binding experiments, maximal binding of D15107 was slightly higher than C9401 or D12092 (Figure 1).

Binding properties of these mAbs were also examined using CHO cells stably expressing hAQP4 (Supporting Information Figure S1A). When cells expressing the M23 isoform alone

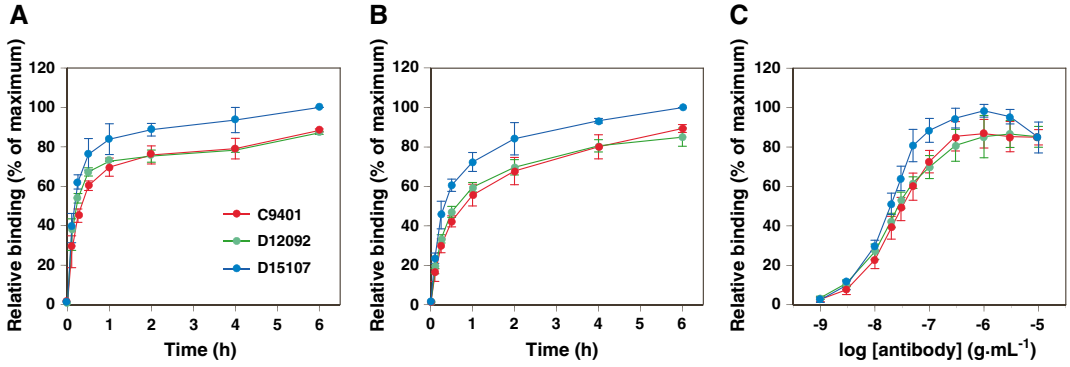

Figure 1

Binding of the mAbs to hAQP4 M23 expressed on the envelope of budded baculovirus. (A and B) Time course of binding of 300 $ng \cdot mL^{-1}$ of C9401, D12092 and D15107 at room temperature (A) or at 4°C (B). Bound antibodies were measured by ELISA and estimated as percent of maximal binding of D15107 at each temperature. Values are means ± SD of three independent experiments performed in duplicate. (C) Concentration–response binding of C9401, D12092 and D15107 at 4°C overnight. Bound antibodies were measured by ELISA and estimated as percent of maximal binding of D15107. Values are means ± SD of four independent experiments performed in duplicate.

Table 1

Binding properties of original and chimeric monoclonal antibodies against the extracellular domains of human aquaporin-4 M23 expressed on budded baculovirus determined by ELISA

	EC_{50} (pM)		
	C9401	D12092	D15107
Original	166 ± 29.7	132 ± 29.7	126 ± 12.6
Chimeric	927 ± 76.4	1670 ± 506	780 ± 56.9

Values were means ± SD of four independent experiments.

(hAQP4-M23) and fixed with 4% PFA were used without permeabilization, all three antibodies showed similar binding patterns, which were bell-shaped, with similar EC_{50} values (Figure 2A–C, green, and Table 2). Initially, binding of each antibody increased as concentrations of mAbs were raised to 100–300 ng · mL^{-1}, followed by gradually reducing their binding to approximately 51–55% of maximal binding at higher concentrations of mAbs, up to ~10 μg · mL^{-1}. Similar to the binding of these antibodies to hAQP4-M23 cells, those to cells expressing both M1 and M23 (hAQP4-M1/M23) were also bell-shaped (Supporting Information Figure S3A), although the avidities (Table 2) were 3.1–5.4-fold lower than those observed in hAQP4-M23 cells. As determined by flow cytometry using CHO cells transiently transfected with AQP4 expression constructs in a previous report (Miyazaki *et al.*, 2013), D15107 was the only antibody that could concentration-dependently bind to 4% PFA-fixed CHO cells stably expressing mouse AQP4 (mAQP4) M23 (Supporting Information Figures S1A, lane 4, and S3B). Although all three mAbs also bound to fixed CHO cells expressing hAQP4 M1 alone (hAQP4-M1), their avidities were extremely low, compared with those for hAQP4-M23, and were too low to be saturated even at a concentration of 30 μg · mL^{-1} (Figure 2A–C). Among them, the binding of D15107 to hAQP4-M1 was slightly higher than those of the other two. Interestingly, when binding experiments were performed using live hAQP4-M1 cells at 37°C for 1 h, these three antibodies showed different binding properties. The binding of C9401 to live hAQP4-M1 cells was almost the same as that to fixed cells (Figure 2A). This was also the case with the binding of D15107 at concentrations up to 1 μg · mL^{-1}; however, it reached a plateau at higher concentrations, the plateau being lower than that to fixed hAQP4-M1 (Figure 2C). In contrast, the binding of D12092 to hAQP4-M1 increased when live cells were used (Figure 2B). These observations indicate that although all mAbs could bind to both M1 and M23 isoforms of hAQP4, they preferentially bound to M23, suggesting that, as with most of the NMO-IgG, they require OAP formation of AQP4 for their antigen recognition. Although D15107 most potently bound to AQP4, in live cells expressing M1 alone, maximal binding of D15107 was limited, especially at high concentrations.

Binding of D15107 strongly induced endocytosis of AQP4

Because the mAbs showed different binding patterns in live hAQP4-M1 cells, we labelled the mAbs with Alexa Fluor 555 and performed live imaging to directly observe their bindings to hAQP4-M1, using a relatively high concentration of each antibody (10 μg · mL^{-1}). Alexa-Fluor-555-labelled D15107 more rapidly bound to hAQP4-M1 (Supporting Information movie 1) than did D12092 (Supporting Information movie 2) or C9401, which was the slowest (Supporting Information movie 3). Interestingly, intracellular accumulation of fluorescence was observed in the cells during the 3 h of treatment with these antibodies, indicating that endocytosis of Alexa-Fluor-555-labelled mAbs via AQP4 occurred in these cells (Supporting Information movies 1–3). Twenty-four hours after incubation, binding of Alexa-Fluor-555-labelled mAbs showed punctate staining patterns, and labelled C9401 and D12092 were still observed on the cell surface, whereas D15107 was mainly localized in the intracellular compartment of the cells, whose outlines were not obvious (Figure 3), suggesting that in these cells, D15107 enhanced endocytosis of AQP4 more strongly than did the other two. To assess to which intracellular compartment the endocytosed AQP4 by treatment with D15107 was transported, we performed Western blotting of lysate extracted from hAQP4-M1 cells treated with D15107 for 24 h. As shown in Figure 4, the level of AQP4 in these cells was significantly reduced, compared with those treated with E5415B (Figure 4A, lanes 2 and 5, and Figure 4B), a mouse-specific mAb that does not bind to hAQP4 (Huang

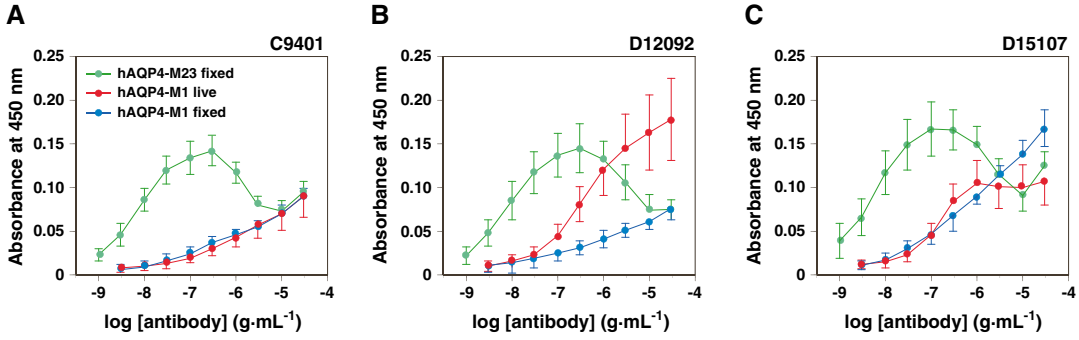

Figure 2

Binding of the mAbs to AQP4 expressed in stable CHO cell lines. (A–C) Concentration-dependent binding of C9401 (A), D12092 (B) and D15107 (C) to fixed CHO cells expressing M23 alone (hAQP4-M23) or M1 alone (hAQP4-M1) at 4°C overnight, or live hAQP4-M1 37°C for 1 h. Values are means ± SD of six independent experiments performed in duplicate.

Table 2

Binding properties of monoclonal antibodies against the extracellular domains of aquaporin-4 expressed on CHO cells determined by ELISA

	EC_{50} (pM)		
Cells	**C9401**	**D12092**	**D15107**
hAQP4-M23	47.6 ± 10.3	50.3 ± 9.12	86.2 ± 23.0
hAQP4-M1/M23	256 ± 29.2	217 ± 27.4	268 ± 45.4
mAQP4-M23	–	–	713 ± 111

Values were means ± SD of six independent experiments.
hAQP4, human aquaporin-4; mAQP4, mouse aquaporin-4.

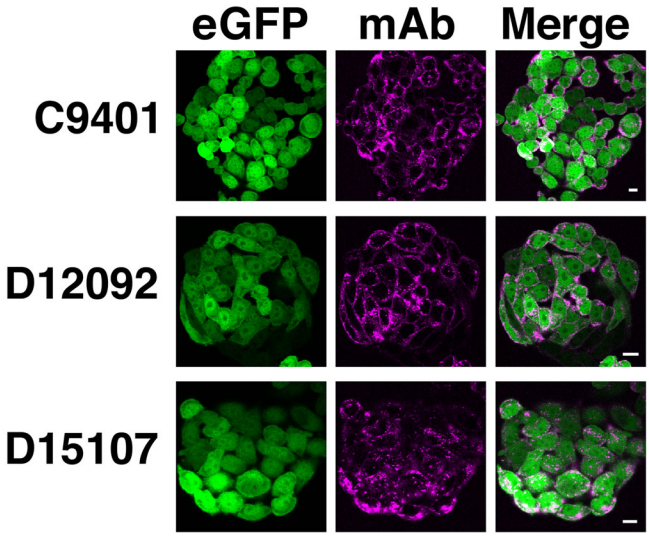

Figure 3

Live imaging of binding of fluorescent-labelled mAbs to hAQP4-M1 cells. Cells were treated with 10 μg · mL^{-1} Alexa-Fluor-555-labelled C9401, D12092 or D15107, and fluorescence of eGFP expressed in hAQP4-M1 cells and mAbs was observed 24 h after incubation. Bar = 10 μm.

et al., unpublished experiments). C9401 also significantly reduced the level of AQP4 in these cells (Figure 4A, lane 3, and Figure 4B), but its effect was weak, compared with that of D15107. The reduction of AQP4 in hAQP4-M1 cells treated with these antibodies was restored by simultaneous treatment with bafilomycin A1, an inhibitor for lysosomal function, indicating that the reduced level of AQP4 following treatment with the mAbs was due to transportation of AQP4 to lysosomes followed by degradation (Figure 4A, lanes 4 and 6, and Figure 4B). All mAbs were also endocytosed in hAQP4-M23, but in contrast to hAQP4-M1 cells, not only C9401 and D12092 but also D15107 stayed on the cell surface even after 24 h of incubation (Supporting Information Figure S4). Consistent with this observation, D15107 did not significantly enhance lysosomal degradation of AQP4 in hAQP4-M23 cells (Supporting Information Figure S5). Taken together, D15107 strongly enhanced endocytosis and lysosomal degradation of AQP4, especially in cells expressing the M1 isoform alone.

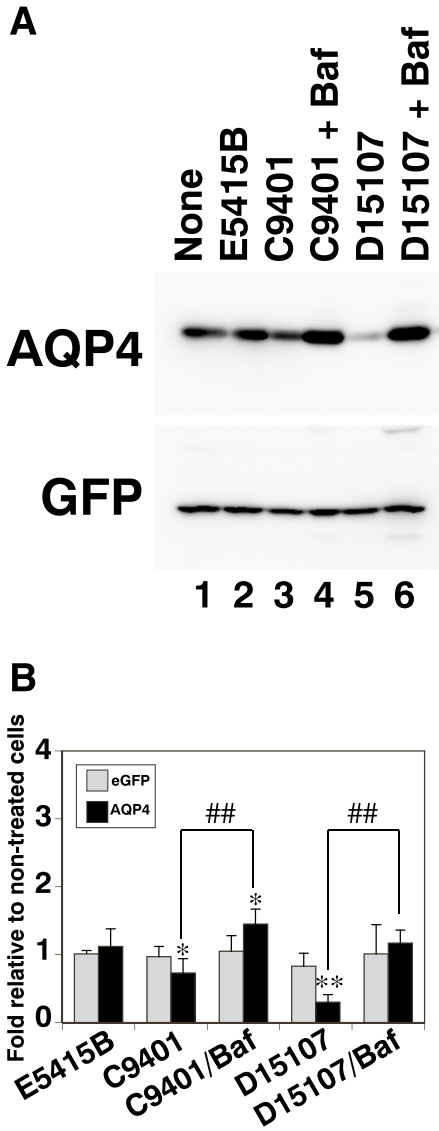

Figure 4

Effect of mAbs on levels of AQP4 in hAQP4-M1 cells. (A) A typical blot is shown. (B) hAQP4-M1 cells were treated with 5 μg · mL^{-1} of C9401 (lanes 3 and 4), D15107 (lanes 5 and 6) or mAQP4-specific E5415B (lane 2) in the absence (lanes 2, 3 and 5) or presence (lanes 4 and 6) of 100 nM bafilomycin A1 at 37°C for 24 h. Amounts of eGFP and AQP4 were determined by Western blotting and estimated as fold relative to non-treated cells (lane 1). Data shown are means ± SD of six independent experiments. ** $P < 0.01$, * $P < 0.05$; significantly different from cells treated with E5415B alone. ## $P < 0.01$; significant effects of bafilomycin A1 treatment; one-way ANOVA with Tukey–Kramer test.

Establishment of chimeric D15107 and its cytoprotective effect against CDC induced by NMO-IgG

To assess potency of D15107 as a new therapeutic drug for NMO, we cloned variable regions of heavy and light chains of D15107 as well as two others, C9401 and D12092, as described in the Methods and Supporting Information Figure S2. Obtained cDNAs for variable regions of heavy and light chains were

connected with constant regions of human IgG1 and Igκ, respectively, and inserted into mammalian expression vectors to establish stable cell lines expressing each chimeric mAb to examine its cytoprotective effect against NMO-IgG-induced CDC. Purified chimeric D15107 was subjected to binding study by ELISA using 96-well plates, where BV expressing hAQP4 M23 was immobilized. As shown in Figure 5A, chimeric D15107 bound to hAQP4 M23 with high avidity (7.8×10^{-10} M, Table 1) compared with recombinant NMO-IgGs cloned from clonally expanded plasma blast populations in the CSF of NMO patients (Crane *et al.*, 2011), although the EC_{50} value was 6.2-fold higher than that of original D15107. This reduction of the avidity by changing to a chimeric antibody, observed in D15107, was also the case with C9401 and D12092, whose chimeric mAbs showed 5.6-fold and 12.6-fold, respectively, lower avidities than did the corresponding original mAbs (Figure 5B and C and Table 1).

Because the chimeric D15107 was found to bind to hAQP4 with high avidity, we next examined whether this antibody would prevent CDC induced by NMO-IgG from patient serum using a CHO cell clone expressing both M1 and M23 isoforms of hAQP4 (hAQP4-M1/M23), which mimics cells endogenously expressing AQP4. Chimeric D15107 ($10\,\mu g \cdot mL^{-1}$, Figure 6B, C-D15107) did not show any CDC in the cells in the presence of 2% rabbit serum (rabbit complement). Purified IgG fractions from NMO patient 1, 3, 4 and 5 ($200–500\,\mu g \cdot mL^{-1}$, Miyazaki *et al.*, 2013) in the presence of 2% rabbit complement increased cell mortality from twofold to threefold, compared with non-treated cells; however, simultaneously added chimeric D15107 at a concentration of $10\,\mu g \cdot mL^{-1}$ completely prevented CDC, although $2\,\mu g \cdot mL^{-1}$ of chimeric D15107 showed little cytoprotective effect (Figure 6A, B, C and D, respectively).

Chimeric D15107 caused no harm to a mouse,s body

To verify the safety of chimeric D15107 *in vivo*, we first injected 1 mg of chimeric D15107 i.p.into 12-week-old female C57BL/6J mice. The injected mice appeared to be healthy and did not show any weight loss, over the 4 days after the injection (Figure 7A). Serum level of chimeric D15107 was approximately $0.5\,mg \cdot mL^{-1}$ on day 2 after injection and lasted until day 4 (Figure 7B). Histological examinations of the kidney, one of the peripheral organs expressing high level of AQP4, from chimeric D15107-injected mice (Figure 7C and D, Supporting Information Figure S6A and B), were indistinguishable from that of age-matched untreated mice (Figure 7F and G, Supporting Information Figure S6C and D), and no obvious AQP4 loss was observed. Furthermore, intra-cerebral injection of chimeric D15107 (5.5 μg) in the presence of human complement did not cause any AQP4 loss in the brain (Figure 7E), whereas a lower dose of E5415A (1 μg), a mAb selectively recognizing the ECDs of mAQP4 (Huang *et al.*, unpublished experiments), clearly produced large AQP4 loss (Figure 7H, asterisk). These observations suggest that chimeric D15107 did not harm either peripheral organs or the brain, after treatment *in vivo*.

Discussion

We have already described mAbs against the ECDs of hAQP4, established using the baculovirus display method (Miyazaki *et al.*, 2013), which displaced binding of NMO-IgG to live hAQP4-M23 cells by administration even at 2 h after incubation with NMO-IgG. These antibodies had subnanomolar EC_{50} values (Figures 1 and 2 and Tables 1 and 2), which represent between 20 to several hundred times higher avidities than those of recombinant NMO-IgGs cloned from clonally expanded plasma blast populations in the CSF of NMO patients (Crane *et al.*, 2011). The recombinant NMO-IgGs prevented the development of NMO lesions in *ex vivo* and *in vivo* models (Tradtrantip *et al.*, 2012), supporting the idea that the mAbs could be a potential therapeutic option for NMO and NMOSD by antagonizing binding of NMO-IgG to AQP4. To evaluate the potency of these mAbs as a therapeutic drug, we constructed chimeric mAbs by cloning of a cDNA fragment encoding variable regions of heavy and light chains from each hybridoma. Among them, chimeric D15107 bound to hAQP4 with the highest avidity and prevented NMO-IgG-induced CDC *in vitro*, even when it was administered to the cells simultaneously with NMO-IgG and complement (Figure 5).

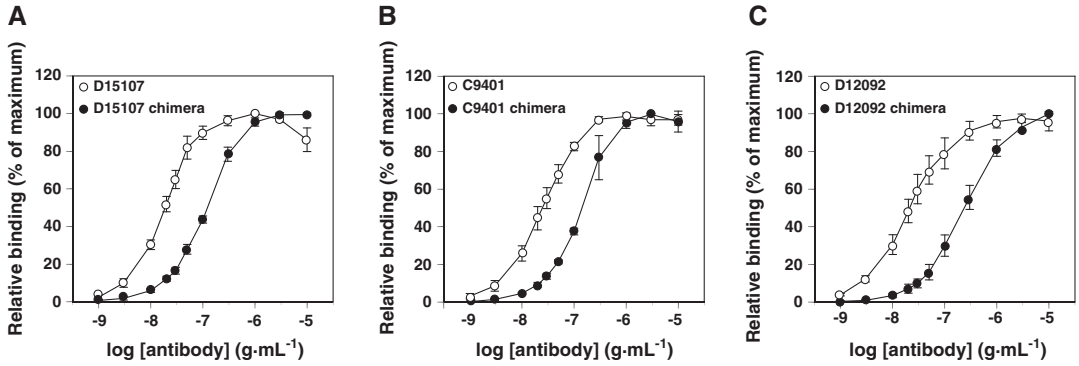

Figure 5

Binding of chimeric mAbs to hAQP4 M23 expressed on the envelope of budded baculovirus. Concentration-dependent binding of original and chimeric D15107 (A), C9401 (B) and D12092 (C) to hAQP4 M23 expressed on the envelope of BV were determined by ELISA at 4°C overnight and shown as percent of maximal binding of each antibody. Data shown are means ± SD of four independent experiments performed in duplicate.

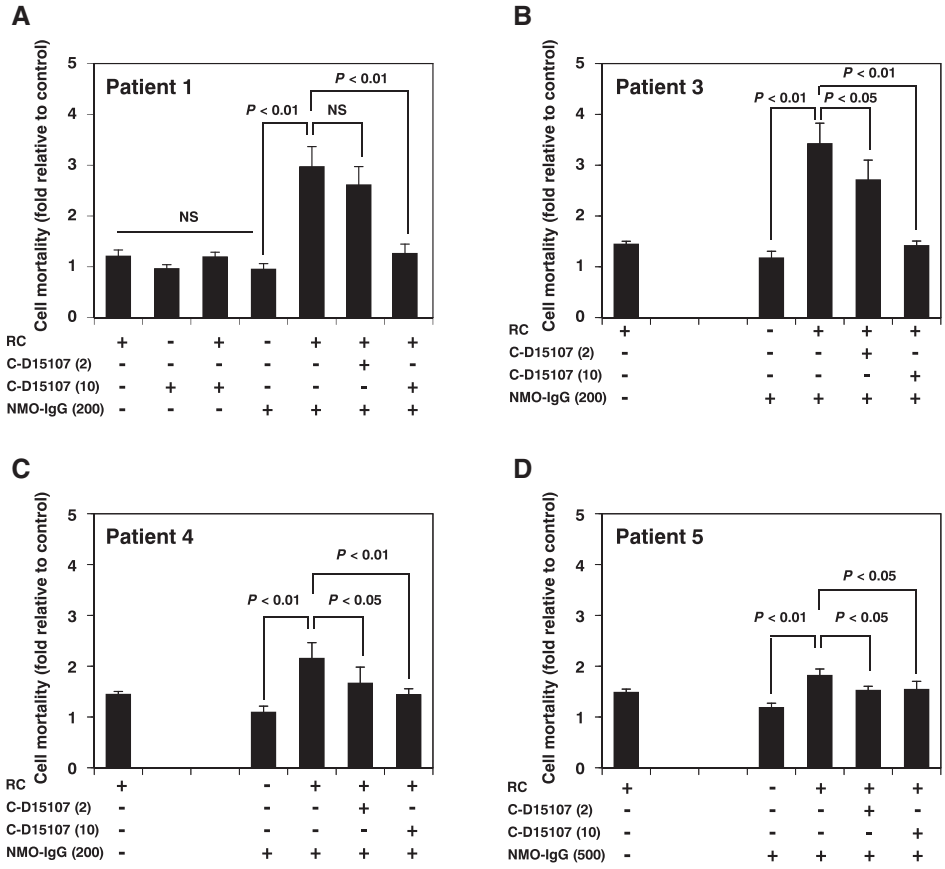

Figure 6

Cytoprotective effect of chimeric D15107 against CDC induced by NMO-IgG. hAQP4-M1/M23 cells were treated with either rabbit complement (RC), 2 or 10 μg · mL^{-1} of chimeric D15107 (C-D15107), or 200–500 μg · mL^{-1} of the purified IgG fractions from patients 1 (A), 3 (B), 4 (C) and 5 (D) described in Miyazaki *et al.* (2013) (NMO-IgG) or their combinations as indicated at 37°C for 2 h. Cell mortalities were determined by LDH assay and estimated as fold relative to non-treated cells (control). Data shown are means ± SD of four independent experiments performed in duplicate. ** $P < 0.01$, * $P < 0.05$; significantly different as indicated; one-way ANOVA with Tukey–Kramer test. NS, not significant.

We observed that the concentration-dependent curves of all mAbs examined were bell-shaped when cells expressing M23 isoform (hAQP4-M23, hAQP4-M1/M23 and mAQP4-M23) were used (Figure 2 and Supporting Information Figure S3). This phenomenon may reflect the requirement of bivalent binding of these mAbs to AQP4 M23 to achieve high avidity. It is notable that AQP4 expressed in hAQP4-M23 and hAQP4-M1/M23 cells was supposed to form OAPs (Yang *et al.*, 1996; Furman *et al.* 2003). The distance between two AQP4 tetramers in an array is close to that between two Fab domains of an antibody. We have directly observed that two Fab domains of C9401 cross-linked two tetramers of AQP4 in an array by high-speed atomic force microscopy (Yamashita *et al.*, unpublished experiments). If this is the case, at low concentrations, all antibodies will concentration-dependently bind to AQP4 in an array by bivalent binding. However, at relatively high concentrations, antibodies binding to AQP4 monovalently, which must be at a much lower avidity for AQP4 than the bivalent one, will appear and increase as the concentration of mAbs becomes higher because of steric hindrance, leading to reduction of bound mAbs at higher concentrations. This scheme would also explain why binding of these mAbs to hAQP4-M1 cells, which have few OAPs, showed much lower avidity than that to hAQP4-M23 or hAQP4-M1/M23, although the primary sequence of the ECDs between M1 and M23 is exactly the same. In hAQP4-M1 cells, it is highly likely that most of the AQP4 tetramers are randomly located with distances between them, not appropriate to achieve bivalent binding of the mAbs. When two tetramers are situated close to each other within an acceptable distance for bivalent binding of the mAbs, the mAbs are able to bind to AQP4. Because the movement of the M1 isoform along the cell surface is much faster than that of the M23 isoform incorporated into an array (Crane *et al.* 2008; 2009), more binding sites for bivalent binding of mAbs must be repeatedly produced in live cells. We observed more binding of D12092 to live hAQP4-M1 cells (Figure 2B), supporting this idea. We also observed that the avidity of D15107 for mAQP4-M23 cells was approximately 10 times lower than that for hAQP4-M23 cells, which is probably due to decreased intrinsic affinity between the paratope and epitope. But it was higher than that for hAQP4-M1 cells, also supporting the bivalent binding hypothesis. However, we cannot exclude the possibility that the mAbs recognize a particular three-dimensional conformation formed by the three extracellular loops of AQP4 and that this conformation is changed when AQP4 is incorporated into an array, leading to drastically reduced intrinsic affinity between the paratope and epitope.

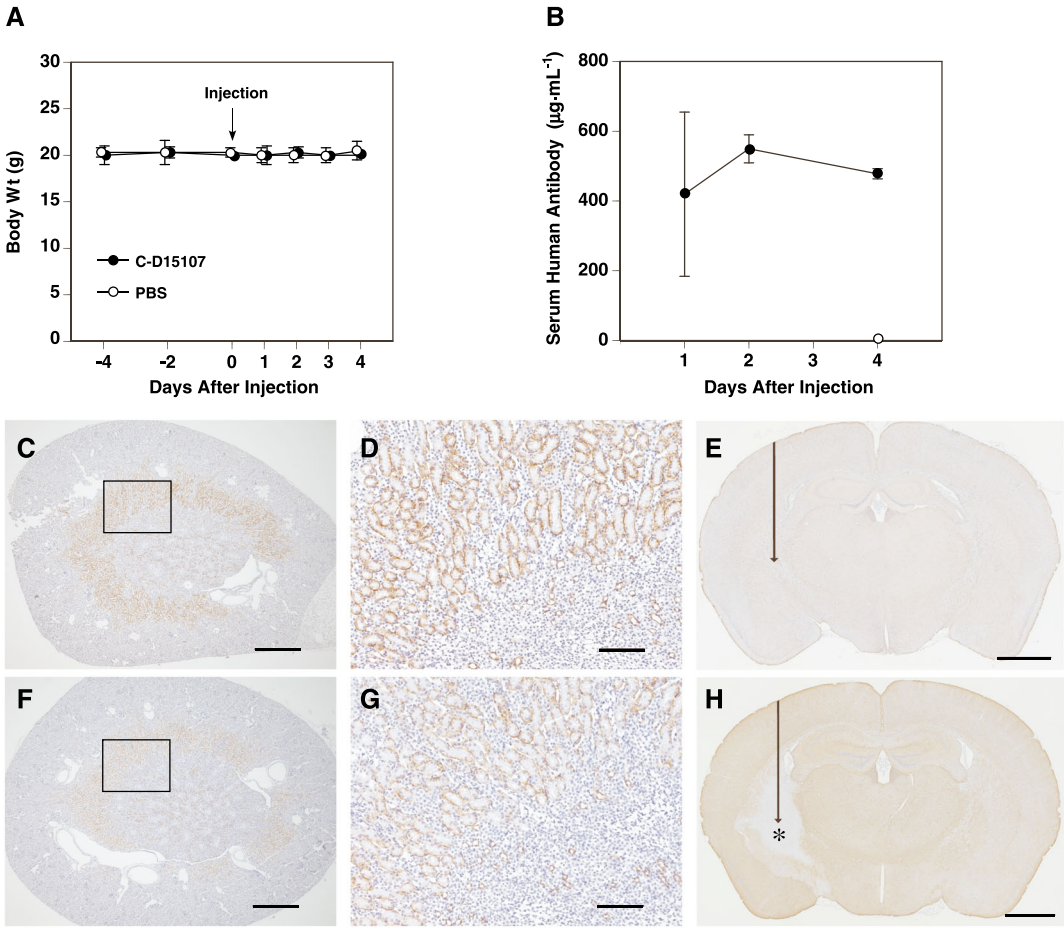

Figure 7

Injection (i.p. or intra-cerebral) of chimeric D15107 into mice. (A) Body weights of mice injected i.p. with 1 mg of chimeric D15107 ($n = 3$) or PBS ($n = 4$). (B) Serum levels of chimeric D15107 in mice after i.p. injection ($n = 3$ for each time point) determined by ELISA. Concentrations of the antibody detected with secondary anti-human IgG antibody were below the detectable level in mice injected with PBS ($n = 4$). One out of three mice on day 1 of post-injection showed exceptionally lower antibody concentration (153 $\mu g \cdot mL^{-1}$), compared with the other two (599 and 506 $\mu g \cdot mL^{-1}$), which caused marked variability. (C, D, F and G) Histology of kidneys from mice injected i.p. with chimeric D15107 (C and D) or age-matched untreated mice (F and G). Three mice were used for each group and produced similar results. D and G are magnified images of C and F respectively. Magnified regions are indicated with boxes. Representative images are shown. Bar = 500 and 100 μm for C, F and D, G respectively. (E and H) Histology of brains from mice intra-cerebrally injected with 5.5 μg of chimeric D15107 (E) or 1 μg of E5415A (F), a mouse-selective anti-AQP4 extracellular domain antibody (Huang *et al.*, unpublished experiments), simultaneously with human complement (5%). The direction and the site of injection are indicated with an arrow. AQP4 loss (* in H) was observed only in the brain injected with E5415A. Three mice were used for each group, and near identical results were obtained. Representative images are shown. Bar = 1 mm.

Among the mAbs we established, D15107 not only bound to AQP4 more potently than the other two mAbs but also strongly enhanced endocytosis and transportation of AQP4 to lysosomes, especially in hAQP4-M1 cells, which reduced the amounts of AQP4 on the cell surface (Figures 3 and 4). We observed that when a binding experiment was performed using live hAQP4-M1 cells, binding of D15107 reached a plateau at high concentrations. The plateau was lower than that to fixed hAQP4-M1 cells (Figure 2C) probably because of the endocytosis enhanced by D15107 and the reduction in AQP4 on the cell surface in live cells. The ability of D15107 to decrease the number of cell-surface AQP4 by endocytosis is an advantage, in terms of preventing CDC induced by NMO-IgG. According to the phenotypes of AQP4 knockout mice (Ma *et al.*, 1997), transient loss of AQP4 on the cell surface by antibody-induced endocytosis does not seem harmful. However, Hinson *et al.* (2008) proposed a pathomechanism of NMO, where loss of the excitatory amino acid transporter 2 on the surface of astrocytes accompanied the endocytosis of AQP4, disrupting glutamate homeostasis. For this reason, we assessed the effects of i.p. injection of chimeric D15107 and found no obvious abnormality or toxicity (Figure 7 and Supporting Information Figure S6). Consistent with this observation, intravenously injected recombinant NMO-IgG did not show any toxicity in mice (Ratelade *et al.*, 2011), although it still induced CDC and ADCC. This recombinant NMO-IgG caused NMO-like lesions in mouse brain when it was intra-cerebrally injected with human complement (Saadoun *et al.*, 2010). We also obtained a similar result when E5415A, a mAb developed

against the ECDs of mAQP4 which induced CDC and ADCC (Huang *et al.*, unpublished experiments), was used (Figure 7H). In contrast, chimeric D15107 did not induce NMO-like lesions, even in a higher dose (Figure 7E), indicating that D15107 is a non-pathogenic antibody. However, high-avidity, chimeric mAbs that enhance little endocytosis of AQP4, such as C9401 and D12092, should also be considered.

All our mAbs were sensitive to amino acid substitutions in loop A, the most divergent extracellular loop between hAQP4 and mAQP4, probably because the mAbs had been established by immunizing mice with a wild-type genetic background in terms of the AQP4 gene with hAQP4 M23 expressed on BV (Miyazaki *et al.*, 2013). In fact, the variable regions of all three light chains are predicted to be derived from the same V exon (Supporting Information Figure S2). To establish much better antibodies against the ECDs of hAQP4 with a variety of epitopes as well as with higher avidities, which can be applied to the treatment of NMO/NMOSD, we are currently immunizing mice with an AQP4 knockout background (Ikeshima-Kataoka *et al.* 2013) as hosts.

In conclusion, we have developed non-pathogenic, high-avidity, chimeric antibodies against the ECDs of hAQP4. We propose that they are potential therapeutic drugs for preventing the progress and recurrence of NMO/NMOSD.

Acknowledgements

The authors thank Ms Wakami Goda, Ms Manae Imamura and Mr Yasuhiro Furuuchi for invaluable help; Dr Dovie Wylie, Ms Michi Enoto, Ms Yuri Atobe, Ms Yoshiko Yagyu and Ms Yoko Yamamoto for expert assistance; Mr Simon Chau for reviewing the manuscript; Collaborative Research Resources, School of Medicine, Keio University for technical assistance and all members of the Department of Pharmacology, School of Medicine, Keio University for cooperation.

This work was supported by grants from Japan Society for the Promotion of Science Grant-in-Aid for Scientific Research (C) (22590940) (YA), Grant-in-Aid for Challenging Exploratory Research (25670425) (YA), Keio Gijuku Academic Development Funds (YA), Global Center of Excellence Program for Humanoid Metabolomic Systems Biology of the Ministry of Education, Culture, Sports, and Technology (A13) (MEXT) of Japan, Grant-in-Aid for Scientific Research (B) (21390061) (MY), the Japan New Energy and Industrial Technology Development Organization (NEDO, P08005) (MY), Keio University Special Grant-in-Aid for Innovative Collaborative Research Projects (MY), the NEAT project of the Japan New Energy and Industrial Technology Development Organization (NEDO, P06009) (TH), the Grants-in-Aid for Scientific Research (KAKENHI) from the Ministry of Education, Science and Technology of Japan (22229008) (KF), and the Grants-in-Aid for Scientific Research (Research of Neuroimmunological Diseases) from the Ministry of Health, Welfare and Labor of Japan (201324020A) (KF).

Author contributions

Y. A., H. I., M. Y., T. H., K. F., T. S. and Y. T. designed the study; K. M-K., Y. T., P. H., O. K-A., H. I., K. K., K. M. and Y. A. performed the experiments; T. M. contributed essential specimens and K. M-K., Y. T., Y. A. and M. Y. wrote the manuscript.

Conflict of interest

Kazuo Fujihara serves on Scientific Advisory Boards for Bayer Schering Pharma, Biogen Idec, Mitsubishi Tanabe Pharma Corporation, Novartis Pharma, Chugai Pharmaceutical, Ono Pharmaceutical, Nihon Pharmaceutical, Merck Serono, Alexion Pharmaceuticals, Medimmune and Medical Review, has received funding for travel and speaker honoraria from Bayer Schering Pharma, Biogen Idec, Eisai Inc., Mitsubishi Tanabe Pharma Corporation, Novartis Pharma, Astellas Pharma Inc., Takeda Pharmaceutical Company Limited, Asahi Kasei Medical Co., Daiichi Sankyo and Nihon Pharmaceutical and has received research support from Bayer Schering Pharma, Biogen Idec Japan, Asahi Kasei Medical, The Chemo-Sero-Therapeutic Research Institute, Teva Pharmaceutical, Mitsubishi Tanabe Pharma, Teijin Pharma, Chugai Pharmaceutical, Ono Pharmaceutical, Nihon Pharmaceutical and Genzyme Japan. Katsushi Koda and Katsuyuki Mitomo are on the staff of Perseus Proteomics Inc. The other authors declare no conflicts of interest.

References

Abe Y, Kita Y, Niikura T (2008). Mammalian Gup1, a homolog of *Saccharomyces cerevisiae* glycerol uptake/transporter 1, acts as a negative regulator for N-terminal palmitoylation of Sonic hedgehog. FEBS J 275: 318–331.

Alexander SPH, Benson HE, Faccenda E, Pawson AJ, Sharman JL, Catterall WA *et al.* (2013). The Concise Guide to PHARMACOLOGY 2013/14: Ion Channels. Br J Pharmacol 170: 1607–1651.

Crane JM, Van Hoek AN, Skach WR, Verkman AS (2008). Aquaporin-4 dynamics in orthogonal arrays in live cells visualized by quantum dot single particle tracking. Mol Biol Cell 19: 3369–3378.

Crane JM, Bennett JL, Verkman AS (2009). Live cell analysis of aquaporin-4 M1/M23 interactions and regulated orthogonal array assembly in glial cells. J Biol Chem 284: 35850–35860.

Crane JM, Lam C, Rossi A, Gupta T, Bennett JL, Verkman AS (2011). Binding affinity and specificity of neuromyelitis optica autoantibodies to aquaproin-4 M1/M23 isoforms and orthogonal arrays. J Biol Chem 286: 16516–16524.

Fujihara K (2011). Neuromyelitis optica and astrocytic damage in its pathogenesis. J Neurol Sci 306: 183–187.

Furman CS, Gorelick-Feldman DA, Davidson KGV, Yasumura T, Neely JD, Agre P *et al.* (2003). Aquaproin-4 square array assembly: opposing actions of M1 and M23 isoforms. Proc Natl Acad Sci U S A 100: 13609–13614.

Hinson SR, Roemer SF, Lucchinetti CF, Fryer JP, Kryzer TJ, Chamberlain JL *et al.* (2008). Aquaporin-4-binding autoantibodies in patients with neuromyelitis optica impair glutamate transport by down-regulating EAAT2. J Exp Med 205: 2473–2481.

Ikeshima-Kataoka H, Abe Y, Abe T, Yasui M (2013). Immunological function of aquaporin-4 in stab-wounded mouse brain in concert with a pro-inflammatory cytokine inducer, osteopontin. Mol Cell Neurosci 56: 65–75.

Jarius S, Wildemann B, Paul F (2014). Neuromyelitis optica: clinical features, immunopathogenesis and treatment. Clin Exp Immunol 176: 149–164.

Kilkenny C, Browne W, Cuthill IC, Emerson M, Altman DG (2010). Animal research: reporting *in vivo* experiments: the ARRIVE guidelines. Br J Pharmacol 160: 1577–1579.

Lennon VA, Wingerchuk DM, Kryzer TJ, Pittock SJ, Lucchinetti CF, Fujihara K *et al.* (2004). A serum autoantibody marker of neuromyelitis optica: distinction from multiple sclerosis. Lancet 364: 2106–2112.

Lennon VA, Kryzer TJ, Pittock SJ, Verkman AS, Hinson SR (2005). IgG marker of optic-spinal multiple sclerosis binds to the aquaporin-4 water channel. J Exp Med 202: 473–477.

Lu M, Lee MD, Smith BL, Jung JS, Agre P, Verdijk MAJ *et al.* (1996). The human *AQP4* gene: definition of the locus encoding two water channel polypeptides in brain. Proc Natl Acad Sci U S A 93: 10908–10912.

Lucchinetti CF, Guo Y, Popescu BF, Fujihara K, Itoyama Y, Misu T (2014). The pathology of an autoimmune astrocytopathy: lessons learned from neuromyelitis optica. Brain Pathol 24: 83–97.

Ma T, Yang B, Gillespie A, Carlson EJ, Epstein CJ, Verkman AS (1997). Generation and phenotype of a transgenic knockout mouse lacking the mercurial-insensitive aquaporin-4. J Clin Invest 100: 957–962.

McGrath J, Drummond G, McLachlan E, Kilkenny C, Wainwright C (2010). Guidelines for reporting experiments involving animals: the ARRIVE guidelines. Br J Pharmacol 160: 1573–1576.

Miyazaki K, Abe Y, Iwanari H, Suzuki Y, Kikuchi T, Ito T *et al.* (2013). Establishment of monoclonal antibodies against the extracellular domain that block binding of NMO-IgG to AQP4. J Neuroimmunol 260: 107–116.

Nicchia GP, Mastrototaro M, Rossi A, Pisani F, Tortorella C, Ruggieri M *et al.* (2009). Aquaporin-4 orthogonal arrays of particles are the target for neuromyelitis optica autoantibodies. Glia 57: 1363–1373.

Pawson AJ, Sharman JL, Benson HE, Faccenda E, Alexander SP, Buneman OP *et al.* (2014). The IUPHAR/BPS Guide to PHARMACOLOGY: an expert-driven knowledge base of drug targets and their ligands. Nucleic Acids Res 42 (Database Issue): D1098–D1106.

Pisani F, Mastrototaro M, Rossi A, Nicchia GP, Tortorella C, Ruggieri M *et al.* (2011). Identification of two major conformational aquaporin-4 epitopes for neuromyelitis optica autoantibody binding. J Biol Chem 286: 9216–9224.

Pisani F, Sparaneo A, Tortorella C, Ruggieri M, Trojano M, Mola MG *et al.* (2013). Aquaproin-4 autoantibodies in neuromyelitis optica: AQP4 isoform-dependent sensitivity and specificity. PLoS One 8: e79185.

Ramadhanti J, Huang P, Kusano-Arai O, Iwanari H, Sakihama T, Misu T *et al.* (2013). A novel monoclonal antibody against the C-terminal region of aquaporin-4. Monoclon Antib Immuodiagn Immunother 32: 270–276.

Ratelade J, Bennett JL, Verkman AS (2011). Intravenous neuromyelitis optica autoantibody in mice targets aquaporin-4 in peripheral organs and area postrema. PLoS One 6: e27412.

Rossi A, Pisani F, Nicchia GP, Svelto M, Frigeri A (2010). Evidences for a leaky scanning mechanism for the synthesis of the shorter M23 protein isoform of aquaporin-4 Implication in orthogonal array formation and neuromyelitis optica. J Biol Chem 285: 4562–4569.

Saadoun S, Waters P, Bell BA, Vincent A, Verkman AS, Papadopulos MC (2010). Intra-cerebral injection of neuromyelitis optica immunoglobulin G and human complement produces neuromyelitis optica lesions in mice. Brain 133: 349–361.

Saitoh R, Ohtomo T, Yamada Y, Kamada N, Nezu J-I, Kimura N *et al.* (2007). Viral envelope protein gp64 transgenic mouse facilitates the generation of monoclonal antibodies against exogenous membrane proteins displayed on baculovirus. J Immunol Methods 322: 104–117.

Schaefer JV, Honegger A, Plückthun A (2010). Construction of scFv fragment from hybridoma or spleen cells by PCR assembly. In: Kontermann R, Dübel S (eds). Antibody Engineering volume 1 2nd edition. Springer: Berlin Heidelberg, pp. 21–44.

Strebe N, Breitling F, Moosmayer D, Brocks B (2010). Cloning of variable domains from mouse hybridoma. In: Kontermann R, Dübel S (eds). Antibody Engineering volume 1 2nd edition. Springer: Berlin Heidelberg, pp. 3–14.

Suzuki H, Nishikawa K, Hiroaki Y, Fujiyoshi Y (2008). Formation of aquaporin-4 arrays is inhibited by palmitoylation of N-terminal cysteine residues. Biochim Biophys Acta 1778: 1181–1189.

Tradtrantip L, Zhang H, Saadoun S, Phuan P-W, Lam C, Papadopoulos MC *et al.* (2012). Anti-aquaporin-4 monoclonal antibody blocker therapy for neuromyelitis optica. Ann Neurol 71: 314–322.

Trebst C, Jarius S, Berthele A, Paul F, Schippling S, Wildemann B *et al.* (2014). Update on the diagnosis and treatment of neuromyelitis optica: recommendations of neuromyelitis optica study group. J Neurol 261: 1–16.

Yang B, Brown D, Verkman AS (1996). The mercurial insensitive water channel (AQP-4) forms orthogonal arrays in stably transfected Chinese hamster ovary cells. J Biol Chem 271: 4577–4580.

Supporting information

Additional Supporting Information may be found in the online version of this article at the publisher's web-site:

http://dx.doi.org/10.1111/bph.13340

Table S1 Primers used to clone variable regions of mAb heavy chains.

Table S2 Primers used to clone variable regions of mAb light chains.

Figure S1 Establishment of CHO-cell clones stably expressing AQP4.

Figure S2 Primary sequences of variable region of mAbs against hAQP4 ECDs.

Figure S3 Binding of the mAbs to CHO-cell lines expressing AQP4.

Figure S4 Live imaging of binding of fluorescent labeled mAbs to hAQP4-M23.

Figure S5 Effect of mAbs on level of AQP4 in CHO-cell clones expressing hAQP4.

Figure S6 Hematoxylin and eosin staining of kidney sections.